



Bistable turbulence in strongly magnetised plasmas with a sheared mean flow

Nicolas Christen ^{1,2,†}, M. Barnes ^{1,3}, M.R. Hardman ¹ and
A.A. Schekochihin ^{1,4}

¹Rudolf Peierls Centre for Theoretical Physics, University of Oxford, Oxford OX1 3PU, UK

²Lincoln College, Oxford OX1 3DR, UK

³University College, Oxford OX1 4BH, UK

⁴Merton College, Oxford OX1 4JD, UK

(Received 8 February 2022; revised 8 July 2022; accepted 11 July 2022)

The prevailing paradigm for plasma turbulence associates a unique stationary state with given equilibrium parameters. We report the discovery of bistable turbulence in a strongly magnetised plasma with a sheared mean flow. Two distinct states, obtained with identical equilibrium parameters in first-principle gyrokinetic simulations, have turbulent fluxes of particles, momentum and energy that differ by an order of magnitude – with the low-transport state agreeing with experimental observations. Occurrences of the two states are regulated by the competition between an externally imposed mean flow shear and ‘zonal’ flows generated by the plasma. With small turbulent amplitudes, zonal flows have little impact, and the mean shear causes turbulence to saturate in a low-transport state. With larger amplitudes, the zonal shear can (partially) oppose the effect of the mean shear, allowing the system to sustain a high-transport state. This poses a new challenge for research that has so far assumed a uniquely defined turbulent state.

Key words: fusion plasma, plasma nonlinear phenomena, plasma simulation

1. Introduction

Turbulence is a common feature of magnetised plasmas, appearing in systems as varied as the solar wind, astrophysical accretion disks and laboratory plasmas. According to the most common paradigm for such systems, a unique stationary turbulent state can be identified given a certain stirring mechanism and a set of equilibrium plasma parameters. Multistable solutions – for which identical parameters admit distinct turbulent states – are known to occur in neutral fluids (Snedeker & Donaldson 1966; Burggraf & Foster 1977; Schmucker & Gersten 1988), where they are associated with bifurcations and hysteretic behaviour (Shtern & Hussain 1993; Ravelet *et al.* 2004). Multistability has also been reported in weakly magnetised systems of charged fluids (Simitiev & Busse 2009; Latter & Papaloizou 2012). In this work, we report the discovery of bistable turbulence in a strongly magnetised plasma, using direct numerical simulations. We find that bistability arises in such a plasma through the interplay of two crucial mechanisms: an externally

† Email address for correspondence: nicolas.christen@physics.ox.ac.uk

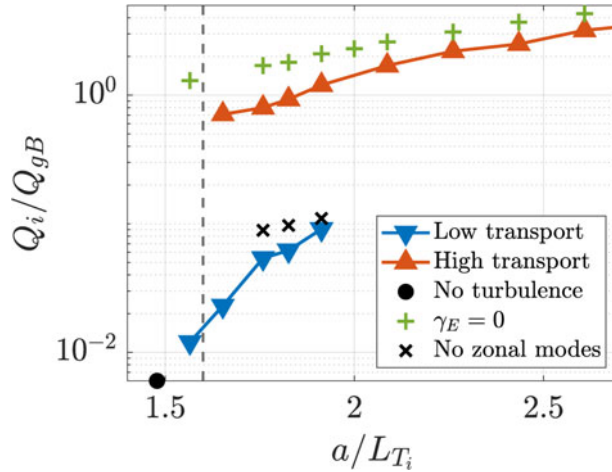


FIGURE 1. Dependence of the turbulent ion heat flux on the inverse ion-temperature-gradient scale length. In the simulations labelled by green ‘+’ signs, the externally imposed mean flow shear was set to zero. For all other simulations, $\gamma_E = -0.079$. Zonal modes are artificially zeroed out in simulations labelled by black crosses. The black circle denotes a simulation where amplitudes decay with time and no saturated turbulent state is observed. The dashed line marks the temperature gradient below which there is no effective linear instability ($\langle \gamma \rangle_t < 0$) in the presence of mean flow shear.

imposed mean flow shear and self-generated ‘zonal’ flows. Our observations are made in a toroidal geometry typically encountered in magnetic-confinement-fusion experiments, although the results may be generalisable to other systems.

Previous studies have already established that sheared flows play an important role in regulating turbulence. In the absence of an externally imposed mean flow shear, the plasma is known to generate sheared ‘zonal’ flows spontaneously, contributing to the saturation of turbulence (Biglari, Diamond & Terry 1990; Dimits *et al.* 2000; Rogers, Dorland & Kotschenreuther 2000; Diamond *et al.* 2005; Colyer *et al.* 2017; van Wyk *et al.* 2017; Ivanov *et al.* 2020). So far, it is therefore usually assumed that the effect of zonal flows is to suppress turbulence. When a mean flow shear is imposed, it provides an additional mechanism for suppressing turbulence. Specifically, the shear in the mean flow perpendicular to the magnetic field has been found to reduce turbulent fluctuations (Waelbroeck & Chen 1991; Artun & Tang 1992; Dimits *et al.* 1996; Synakowski *et al.* 1997; Casson *et al.* 2009; Mantica *et al.* 2009; Highcock *et al.* 2010; Barnes *et al.* 2011; Highcock *et al.* 2012; Schekochihin, Highcock & Cowley 2012; van Wyk *et al.* 2016, 2017). It has also been shown that the effect of the mean shear weakens away from marginal stability (Fox *et al.* 2017; van Wyk *et al.* 2017).

Here, we find that the transition from turbulent states where the mean shear plays an essential role to states where it appears to matter only marginally is characterised by a discontinuous jump in the level of turbulent transport. Most importantly, we show that, in a region of parameter space near this transition, two distinct turbulent states exist with identical equilibrium parameters but dramatically different levels of transport. We find that the presence of strong zonal flows is a feature of higher-transport states – the opposite of what is usually assumed. The main result is presented in figure 1.

This discovery has important implications for research in nuclear fusion. In experiments, turbulent fluxes are set by the external injection of particles, heat and momentum

into the plasma, with profile gradients evolving until a stationary state is reached. However, because of computational cost, direct numerical simulations only consider a small fraction of the device's volume, in which they solve the inverse problem: for given local equilibrium quantities (e.g. profile gradients), the simulations determine the associated turbulent fluxes. The flux-to-gradient problem and its inverse can be considered equivalent if a one-to-one correspondence exists between the turbulent transport and the equilibrium parameters. Our work shows that this correspondence is not always one-to-one, which poses a challenge for modelling transport – and thus for designing future fusion devices. Finally, bistability has some remarkable consequences, such as the possibility for bifurcations of turbulent transport and gradient-relaxation cycles to develop (these have previously been considered in the absence of mean flow shear Peeters *et al.* 2016).

2. Modelling plasmas with a sheared mean flow

We consider equilibrium parameters obtained from a fusion experiment conducted at the Joint European Torus facility (discharge no. 68448 Siren *et al.* 2019). The plasma is confined by magnetic fields that trace out nested toroidal surfaces, with the equilibrium density and temperature staying constant along the field lines. External heating sources sustain an ion temperature gradient between the hotter core and the colder edge of the plasma, which then drives the dominant linear instability (Romanelli 1989; Cowley, Kulsrud & Sudan 1991). A sheared mean toroidal flow is generated by injecting beams of neutral hydrogenic atoms into the plasma. The ratio of thermal to magnetic pressure is small, so the turbulent fluctuations can be assumed electrostatic. We also neglect any trace impurities in the plasma and only consider two kinetic species – the electrons and the main deuterium ions. The simulations include collisions, as well as a small amount of numerical hyperviscosity (Belli 2006). The numerical parameters used for this work are provided as supplementary material available at <https://doi.org/10.1017/S0022377822000691> alongside the present publication.

The model used for this work is presented in Appendix A. The time evolution of turbulent fluctuations is described by following the approach of local δf -gyrokinetics (Catto 1978; Frieman & Chen 1982; Sugama & Horton 1998; Abel *et al.* 2013). This approximation relies on the scale separations present in the system by defining an asymptotic-expansion parameter $\rho_{*s} = \rho_s/a \ll 1$ for a species s , where ρ_s is the particle's gyroradius around a magnetic field line and a is the minor radius of the device. As a result, the rapid gyromotion of particles can be averaged out. In this approach, the kinetic equation and the quasineutrality condition form a closed system of equations for the fluctuating probability distribution function of charged rings and for the electrostatic potential φ . The system is solved numerically with the code GS2 (Kotschenreuther, Rewoldt & Tang 1995; Barnes *et al.* 2009; Highcock 2012) in a filament-like simulation domain (Beer, Cowley & Hammett 1995) that follows a magnetic field line as it wraps around the torus. The code then computes the turbulent contributions to the heat and momentum fluxes exiting the core of the plasma, which we denote by Q_s and Π_s , respectively. In the following figures, we normalise Q_s to the so-called gyro-Bohm value $Q_{\text{gB}} = \langle |\nabla\psi| \rangle_\psi n_i T_i v_{\text{th},i} \rho_{*s}^2$, where ψ is the poloidal magnetic flux, $\langle \cdot \rangle_\psi$ the average over a magnetic-flux surface, T_i the ion temperature multiplied by the Boltzmann constant k_B , $v_{\text{th},i} = \sqrt{2T_i/m_i}$ the ion thermal speed and m_i the ion mass. The ion temperature gradient is specified through a/L_{T_i} , where L_{T_i} is the local e -folding length scale of T_i . Finally, we denote by γ_E the rate at which the mean flow is sheared across magnetic surfaces, normalised by $v_{\text{th},i}/a$.

When $\gamma_E \neq 0$, linear modes (known as Floquet modes) are advected along the magnetic field lines, passing through regions of the plasma that are alternately stable (inboard of the torus) and unstable (outboard) to the ion temperature gradient (Waelbroeck & Chen 1991). As a consequence, their linear growth rate is time dependent with a Floquet period $T_F = 2\pi\hat{s}/\gamma_E$. Here, \hat{s} (defined in Appendix A) measures how the twisting of magnetic field lines around the torus changes with the minor radius. In the following, we denote the time-averaged growth rate by $\langle\gamma\rangle_t$, and the maximum instantaneous growth rate by γ_{\max} . In this work, the code GS2 was used with an improved algorithm for background flow shear described in McMillan, Ball & Brunner (2019) and Christen, Barnes & Parra (2021), although it has been verified that the same conclusions are reached when using the original algorithm devised by Hammett *et al.* (2006).

3. Two distinct turbulent states

Near marginal stability, we find that two distinct turbulent states can be obtained at identical equilibrium parameters. This is shown in figure 1, where saturated values of Q_i/Q_{GB} are plotted against a/L_{T_i} for a particular value of γ_E . We find that the fluxes computed in the low-transport state match the levels of transport observed in the experiment, while the fluxes computed in the high-transport state differ from it by an order of magnitude. For equilibrium parameters where the two states exist, it is the initial size of the fluctuation amplitudes that determines which state is observed in a simulation. While the impact of initial conditions on gyrokinetic simulations was explored in previous work, such as Pueschel, Kammerer & Jenko (2008), our work is the first to obtain two distinct, saturated and finite-amplitude turbulent states with identical equilibrium parameters. Interestingly, we note that both low-transport and high-transport states can exist above and below the threshold for linear instability. Previous work had already established this for a single, finite-amplitude turbulent state sustained either by a linear instability (known as supercritical turbulence) or by transient linear growth (known as subcritical turbulence Highcock *et al.* 2010; Barnes *et al.* 2011; Schekochihin *et al.* 2012).

The two states observed here are distinguished by significant differences in the amplitudes of their turbulent fluctuations and by the spatial structure of the turbulence. In figure 2, we show a typical snapshot of turbulence in a low-transport state. The contours of the fluctuating electrostatic potential are plotted in the plane perpendicular to the magnetic field at the outboard of the torus. The x coordinate measures the distance along the normal to a magnetic-flux surface and the y coordinate labels the magnetic field lines within the surface. The simulation is done in the frame moving with the mean flow at $x = 0$: the y -component of the mean flow thus has the opposite sign to x . The turbulent eddies feature a clear tilt as they are being sheared by the mean flow, similarly to Shafer *et al.* (2012), van Wyk *et al.* (2016, 2017) and Fox *et al.* (2017). In figure 3, we show consecutive snapshots of turbulence with the same equilibrium parameters as in figure 2, but in the high-transport state: bands of high-amplitude eddies propagate radially across the simulation domain, and eddies do not feature any clear tilt. This intermittent high-transport state is reminiscent of advecting structures reported in McMillan *et al.* (2009), McMillan, Pringle & Teaca (2018) and Chandrarajan Jayalekshmi (2020).

4. The role of zonal modes

We find that the presence of ‘zonal’ modes is a crucial distinguishing feature between the two states. Modes are called zonal when they have no spatial variation other than in the radial (x) direction. They are linearly stable and cannot be sheared by a toroidal mean flow, but they can exchange energy with non-zonal modes via nonlinear interactions. Zonal modes include zonal flows with a shearing rate γ_Z , which can affect the rest of the

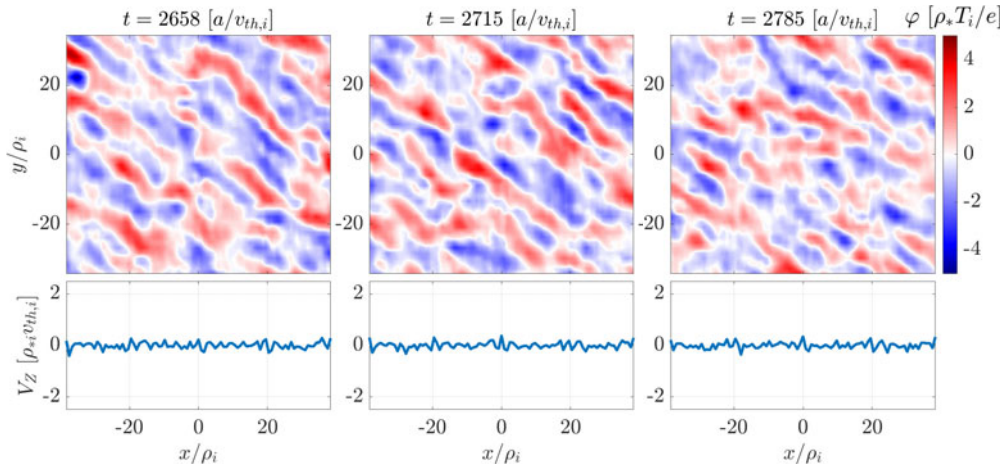


FIGURE 2. Consecutive snapshots of the turbulence in real space for the low-transport state where $a/L_{T_i} = 1.76$ and $\gamma_E = -0.079$. In the top panels, the fluctuating electrostatic potential is plotted at three successive times at the outboard of the torus, in the plane perpendicular to \mathbf{B} . In the bottom panels, the zonal flow is plotted at the same times.

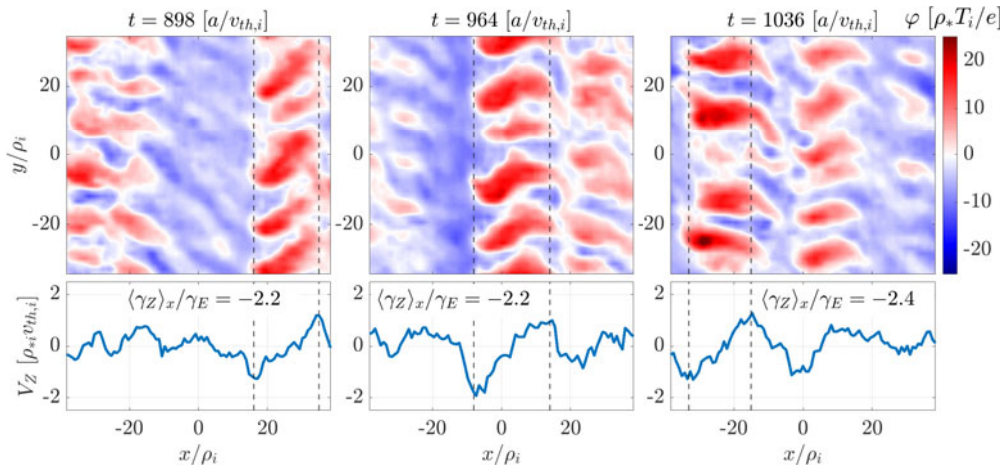


FIGURE 3. Same as figure 2 but for the high-transport state. In the bottom panels, the zonal shear averaged between the two vertical dashed lines is compared with the externally imposed mean flow shear.

turbulence in a manner analogous to the mean flow shear γ_E . The zonal flows are known to develop through a secondary instability of the modes driven unstable by the temperature gradient (Rogers *et al.* 2000; Diamond *et al.* 2005; Ivanov *et al.* 2020).

When the amplitudes of zonal modes become large enough, we find that the zonal shear can compete with, and indeed obviate, the mean flow shear. Such a negation of the equilibrium shear by a zonal shear was already explored in previous work, e.g. McMillan *et al.* (2009, 2018). In the lower panels of figure 3, we plot the zonal flow V_Z ($\propto \partial \varphi_Z / \partial x$ where φ_Z is the zonal part of the potential). We observe radially propagating bands within which the zonal shear γ_Z ($\propto \partial V_Z / \partial x$) is of the same order of magnitude as the background shear γ_E , but carries the opposite sign. In such bands, where the zonal and

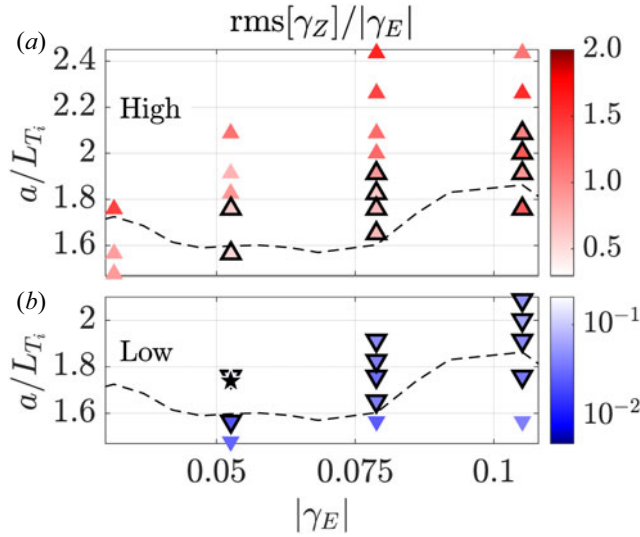


FIGURE 4. Root-mean-square zonal shear versus γ_E for the two turbulent states. High-transport states are shown in (a), and low-transport states in (b). Black-bordered markers indicate parameters at which either a high-transport or a low-transport state can be obtained, depending on the initial size of fluctuation amplitudes. The parameters of the experiment considered here are shown by a black star in (b). The dashed line marks the temperature gradient as a function of γ_E below which turbulence is subcritical ($\langle \gamma \rangle_t < 0$).

mean shears oppose each other, non-zonal fluctuations grow faster and feed the zonal modes nonlinearly, until the system settles in the high-transport state. We also show in figure 1 that the transport obtained in the complete absence of mean flow shear (green ‘+’ symbols) is much closer to the high-transport states than to the low-transport states.

In low-transport states, zonal modes do not seem to play a crucial role for the turbulent dynamics: unlike in the high-transport states, no long-lived structures with γ_Z opposing γ_E are observed. Further evidence of the weaker impact of zonal modes in low-transport states can be seen in simulations where we artificially set zonal modes to zero at every time step, indicated by black crosses in figure 1. Despite this unphysical truncation introduced in the system, and independently of the initial condition, a saturated state is obtained that is – apart from a slight change in the flux – indistinguishable from the low-transport state.

The occurrences of low-transport and high-transport states for a range of mean flow shear rates are shown in figure 4, where we plot the ratio $\text{rms}[\gamma_Z]/\gamma_E$. Here, we define the root mean square of the zonal shear as $\text{rms}[\gamma_Z] = \sqrt{\langle \varphi_Z^2 \rangle_{t,x} / \ell_{x,z}^2}$ and we denote by $\ell_{x,z}$ the radial correlation length of the zonal modes, which we define in Appendix B. As a result of the interplay between the zonal modes and the mean flow, high-transport states are only obtained when the initial fluctuation amplitudes are sufficiently large, or when the fluctuation amplitudes become large enough for the zonal shear to start competing with γ_E (e.g. when a/L_{T_i} is increased or γ_E is decreased past a certain threshold). Figure 4(a) confirms that the magnitude of the zonal shear in the high-transport states is comparable to that of the mean shear and panel (b) indicates that low-transport states only survive when the zonal shear is much smaller than γ_E (roughly by an order of magnitude). This last result could be due to a feedback mechanism whereby even a weak γ_Z can partially oppose γ_E , allowing for larger turbulent amplitudes – and therefore larger zonal modes – to develop.

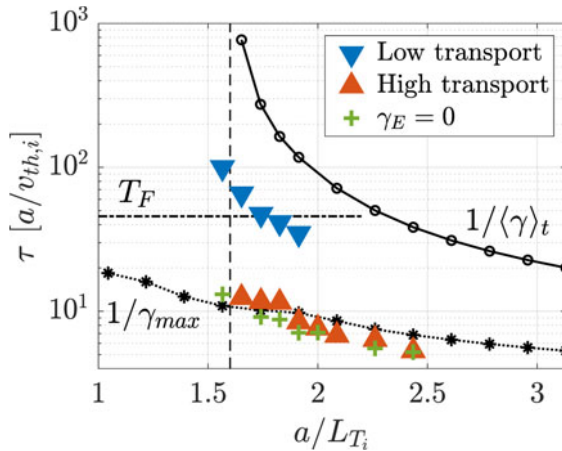


FIGURE 5. Correlation time of turbulent eddies in the low-transport state, high-transport state and in the absence of a mean flow shear. The vertical dashed line marks the temperature gradient below which there is no effective instability in the presence of a mean flow shear, i.e. $\langle\gamma\rangle_t \leq 0$. In the simulations labelled by green ‘+’ signs, the externally imposed mean flow shear was set to zero. For all other simulations, $\gamma_E = -0.079$ was used. Considering other γ_E values leads to similar results.

5. Two correlation time scales

In a saturated turbulent state, the correlation time of the turbulence can be estimated from the gyrokinetic equation by $\tau = [c[\varphi_{\text{NZ}}]_{\text{rms}}/(B\ell_x\ell_y)]^{-1}$, where $[\varphi_{\text{NZ}}]_{\text{rms}}$ is the root-mean-square value of the non-zonal electrostatic potential, ℓ_y is the eddy correlation length in the y direction (defined in Appendix B), c is the speed of light and B is the magnetic field strength. For high-transport states, figure 5 shows that $\tau \sim 1/\gamma_{\text{max}}$, where γ_{max} is the maximum instantaneous linear growth rate in the presence of flow shear (close to the linear growth rate in the absence of flow shear). For low-transport states, $1/\gamma_{\text{max}} < \tau < 1/\langle\gamma\rangle_t$, which may suggest that the average linear growth rate plays a role in setting the saturated turbulent amplitudes in those states. In order for $\langle\gamma\rangle_t$ to be relevant in a turbulent state, eddies must be able to survive longer than a Floquet period, i.e. $\tau \gtrsim T_F$, as is approximately the case for the low-transport states in figure 5. While the competition between zonal and mean flow shear is likely a generic feature of magnetised plasma turbulence, the existence of $\langle\gamma\rangle_t \neq \gamma_{\text{max}}$ requires toroidicity. Further studies are needed to determine if these two distinct growth rates are a necessary feature of the bistable turbulence reported here – and thus if similar bistable states are likely to be found beyond toroidal plasmas.

6. Consequences of bistability

The bistability reported in this work may lead to the existence of bifurcations. As we have argued, low-transport states cease to exist when the fluctuation amplitudes increase past a certain threshold value. If we now consider a plasma in which, instead of being fixed, the temperature gradient is slowly increasing in time, a discontinuous jump will be triggered from a low-transport state to the high-transport branch. The same jump can be triggered by decreasing the mean flow shear in a low-transport state. As shown in figure 4, we observe that the subcritical low-transport states exist closer to marginal stability in the $(\gamma_E, a/L_{T_i})$ plane than the subcritical high-transport states. We attribute this to the intermittent nature of the high-transport state associated with the radially propagating

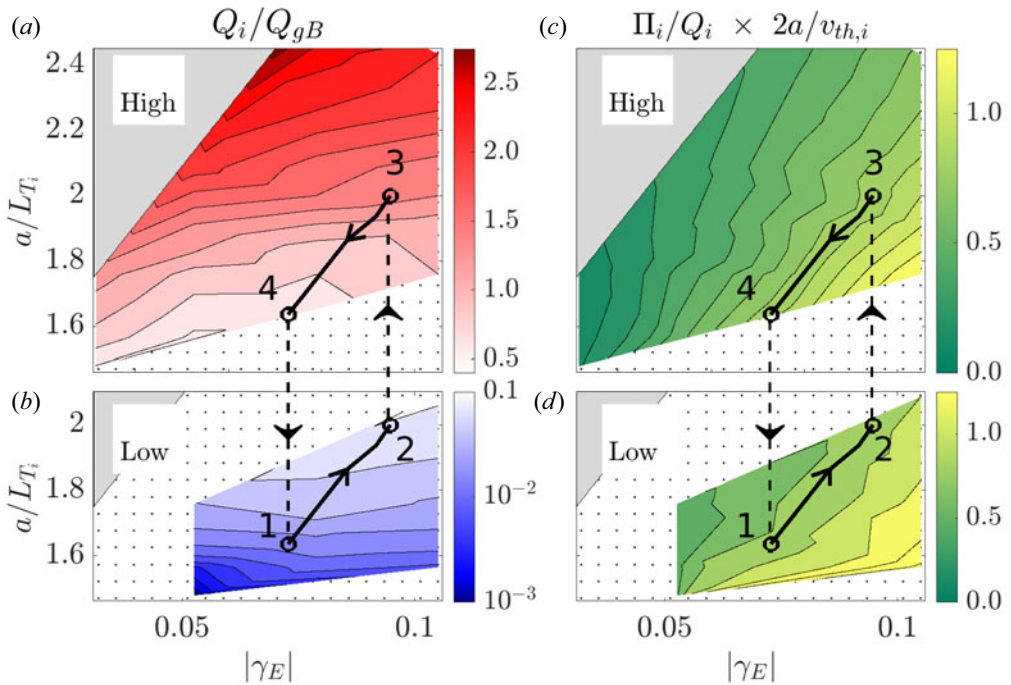


FIGURE 6. Dependence of the ion heat flux (*a,b*) and the momentum-to-heat-flux ratio (*c,d*) on the imposed flow shear and the inverse ion-temperature-gradient scale length. The top panels show results for the high-transport states, the bottom panels for the low-transport states. Dotted areas in the upper (respectively lower) panels indicate areas where no high-transport (respectively low-transport) state could be obtained. The grey areas indicate parameter ranges where no simulations were run. There is a gap between the values of the heat flux obtained in (*a*) and those obtained in (*b*). The path defined by points A, B, C and D gives an example of the successive stages of a gradient-relaxation cycle, when the heat injected into the plasma corresponds to a flux within the aforementioned gap.

bands shown in figure 3. Previous work with neutral fluid flows (Faisst & Eckhardt 2004), accretion disks (Rempel, Lesur & Proctor 2010) and fusion plasmas (Barnes *et al.* 2011; Highcock *et al.* 2011; van Wyk *et al.* 2017) has indeed shown that the survival of subcritical turbulence over long times is compromised by rare, large fluctuations. Similarly to the transition from low to high transport, we argue that subcritical high-transport states can drop to the low-transport branch if the temperature gradient slowly decreases in time. From figure 4, we expect that the same transition could be achieved by increasing the mean flow shear in a subcritical high-transport state.

Existence of bifurcations opens up the possibility for relaxation cycles of the mean gradients to develop. This hinges on two findings that we show in figure 6. First, we observe a significant gap between the highest heat flux obtained in low-transport states and the lowest heat flux obtained in high-transport states. Second, we observe that the ratio of the turbulent momentum flux to heat flux, Π_i/Q_i , is almost identical in the low-transport and high-transport states.

We now consider a thought experiment in which an external power P is injected into the volume bounded by a given magnetic-flux surface of area S , via a beam of neutral atoms with energy E . As is argued in Parra *et al.* (2011), the turbulent heat flux exiting

the magnetic-flux surface is $Q_i \sim P/S$, and $\Pi_i/Q_i \sim E^{-1/2}v_{\text{th},i}/a$. Thus, a given beam configuration corresponds to a unique pair $(Q_i, \Pi_i/Q_i)$. We consider an initial situation where the input power is such that (P, E) corresponds to the levels of turbulent fluxes of a low-transport state (point A in figure 6). From this initial stationary state, we increase P by small successive increments, keeping E fixed. In response, the plasma equilibrium will evolve through a succession of low-transport stationary states with ever larger Q_i , but with Π_i/Q_i staying constant (along the solid arrow up to point B in figure 6).

Above a certain threshold, we find that there is a range of values of P with no corresponding solutions for the turbulent fluxes: in figure 6, these are the powers too high to match the low-transport state at point B, but too low to match the high-transport state at point C. It is then interesting to ask what will happen to a plasma where the input power falls into this gap. One (unexciting) possibility is that an actual solution may exist outside of the region of parameter space explored here, and that the plasma migrates to that solution. Another (more interesting) possibility would be for the temperature gradient to continue increasing until the plasma transitions to a high-transport state (jumping from B to C in figure 6). In this state, the outgoing heat flux is larger than what can be sustained by the external power input, and the temperature gradient starts to flatten. As a/L_{T_i} decreases (from C to D), the turbulent fluctuations remain too large to allow a transition back to a low-transport state. Eventually, a/L_{T_i} becomes too small for the high-transport state to survive, and the system transitions back to the lower state (from D to A). The flux is now too low compared with the power input, so the temperature gradient builds up again, and the cycle repeats itself. In this scenario, no proper steady state is reached when the input power falls within a ‘forbidden’ gap, and the temperature gradient and mean flow shear would experience periodic relaxation cycles.

7. Discussion

We have found that near-marginal turbulence in fusion devices is bistable, and regulated by the competition between external shear and zonal modes. The existence of bistability suggests a new approach to long-standing questions around bifurcations and gradient-relaxation cycles observed in fusion devices (von Goeler, Stodiek & Sauthoff 1974; Wagner *et al.* 1982; Hastie 1997; Connor 1998). This work also presents a new challenge for a research area where the prevailing assumption has been a one-to-one correspondence between plasma parameters and turbulent transport. Further work could focus on how the extent of the bistable region might be modified, for example by exploring the effect of collisions on the saturation of zonal modes (Colyer *et al.* 2017; Weigl *et al.* 2017). Another avenue of interest may be to determine how bistability manifests itself in flux-driven gyrokinetic simulations. Experiments could test the existence of bistability in fusion devices, following a scenario similar to the one described in figure 6. The idea of relaxation cycles discussed in § 6 could be considered in the context of subcritical turbulence, where transitions might occur from a situation with no turbulent transport to a state with a finite level of turbulent transport. Lastly, we note that the details of the plasma analysed here, such as the exact nature of the drive for turbulence and perhaps toroidicity, do not appear to be crucial to our understanding of bistable states: the only requirements we have identified so far are an applied flow shear and the ability of the plasma to generate zonal flows. Therefore, we expect that similar effects may be observed in a variety of systems.

Supplementary material

Supplementary material is available at <https://doi.org/10.1017/S0022377822000691>.

Acknowledgements

The authors are grateful to H. Weisen and P. Sirén for providing the experimental data used in this work. They especially thank F. Parra for his insightful comments on the manuscript. They would also like to thank O. Beeke, J. Parisi and J. Ruiz Ruiz for very fruitful discussions. N.C. was supported by a Berrow Foundation Scholarship, the Steppes Fund for Change and the Fondation H el ene et Victor Barbour. The work of M.H. was funded by EPSRC grant EP/R034737/1, as was, in part, the work of M.B. and A.A.S. Computing resources were provided on the ARCHER High Performance Computer through the Plasma HEC Consortium, EPSRC grant EP/L000237/1 under project e607, on the EUROfusion High Performance Computer (Marconi-Fusion) under the projects FUA34_MULTEI and FUA35_OXGK and on the JFRS-1 supercomputer system at the International Fusion Energy Research Centre's Computational Simulation Centre (IFERC-CSC) at the Rokkasho Fusion Institute of QST (Aomori, Japan) under the project MULTEI.

Editor Paolo Ricci thanks the referees for their advice in evaluating this article.

Declaration of interests

The authors report no conflict of interest.

Appendix A. Gyrokinetic system

In this work, we follow the δf gyrokinetic approach (Catto 1978; Frieman & Chen 1982; Sugama & Horton 1998; Abel *et al.* 2013), which relies on the scale separations present in the plasma to describe the time evolution of turbulent fluctuations. The ratio of gyroradius to machine size $\rho_{*s} = \rho_s/a \ll 1$ for species s is used as the asymptotic-expansion parameter. The minor radius of the device is denoted by a and the gyroradius is given by $\rho_s = |\hat{\mathbf{b}} \times \mathbf{v}/\Omega_s|$, where $\hat{\mathbf{b}}$ is the unit vector in the direction of the magnetic field \mathbf{B} and \mathbf{v} is the velocity of the particle. The gyrofrequency of the particle is $\Omega_s = eZ_s B/m_s c$, where Z_s and m_s are, respectively, the charge number and mass of the particle, e is the elementary charge, and c is the speed of light. The amplitudes of the fluctuations are ordered to be $O(\rho_{*s})$ smaller than the corresponding mean quantities. The turbulent time scale is ordered to be $O(\rho_{*s}^2)$ shorter than the time scale of the evolution of mean plasma parameters, but $O(\rho_{*s}^{-1})$ longer than the Larmor periods of the particles. Moreover, it is assumed that fluctuations can stretch far along magnetic field lines, but that they only span a few gyroradii across field lines. The orderings in time and space can be summarised as

$$\frac{d}{dt} \ln(\delta f_s) \sim \rho_{*s}^{-2} \frac{d}{dt} \ln(F_s) \sim O(\rho_{*s} \Omega_s), \quad (\text{A1})$$

$$\hat{\mathbf{b}} \cdot \nabla \ln(\delta f_s) \sim \rho_{*s} |\nabla \ln(\delta f_s)| \sim |\nabla \ln(F_s)| \sim O(1/a), \quad (\text{A2})$$

where δf_s is the fluctuating part of the distribution function of particles and F_s is their mean distribution function (averaged over the turbulent time scales and over the turbulent length scales across \mathbf{B}). Here, $d/dt = \partial/\partial t + \mathbf{u} \cdot \nabla$ is the convective time derivative with respect to the mean flow \mathbf{u} .

The geometry of the system considered here is typical of magnetic-confinement-fusion experiments. The plasma is confined in a toroidally shaped magnetic cage. The magnetic field lines of this cage wind around the torus, tracing out nested toroidal surfaces, known as magnetic-flux surfaces. The rapid gyromotion about magnetic field lines limits the ability of charged particles to move across these flux surfaces.

We focus on plasmas with a mean flow such that $\rho_{*s} \ll |\mathbf{u}|/v_{th,i} \ll 1$, where $v_{th,i} = \sqrt{2T_i/m_i}$ is the ion thermal speed and T_i is the ion temperature multiplied by the Boltzmann constant k_B . In this ‘intermediate-flow’ ordering, we can neglect the centrifugal force, and the mean flow is purely toroidal (Catto, Bernstein & Tessarotto 1987; Abel *et al.* 2013): $\mathbf{u} = \Omega_\phi R^2 \nabla \phi$ with Ω_ϕ the angular rotation frequency, R the major radius of the torus and ϕ the toroidal angle. It follows that the perpendicular and parallel flow shear rates are related by a geometrical factor, and both can be expressed in terms of the shearing rate $\gamma_E = (r_{\psi,0}/q_0) \partial \Omega_\phi / \partial r_\psi|_{r_{\psi,0}}$, where the subscript ‘0’ denotes quantities evaluated on the flux surface of interest, r_ψ is the half-width of the flux surface at the height of the magnetic axis and the safety factor $q = (2\pi)^{-1} \int_0^{2\pi} d\theta (\mathbf{B} \cdot \nabla \phi) / (\mathbf{B} \cdot \nabla \theta)|_\psi$ is the number of toroidal turns required by a field line to wind once around the torus poloidally. The magnetic shear appearing in § 2 is defined as $\hat{s} = (r_{\psi,0}/q_0) \partial q / \partial r_\psi|_{r_{\psi,0}}$. We further restrict consideration to cases with low thermal-to-magnetic-pressure ratio (plasma beta) and hence only retain electrostatic fluctuations. We neglect all effects associated with impurities in the plasma, and only consider electrons and the main hydrogenic ion species.

After averaging over the rapid gyromotion of particles, the gyrokinetic equation can be written as

$$\begin{aligned} \frac{d\langle \delta f_s \rangle_{R_s}}{dt} + \left(w_\parallel \hat{\mathbf{b}} + \mathbf{V}_{B,s} + \mathbf{V}_{C,s} + \langle \mathbf{V}_E \rangle_{R_s} \right) \cdot \nabla \left(\langle \delta f_s \rangle_{R_s} + \frac{eZ_s \langle \varphi \rangle_{R_s}}{T_s} F_{0,s} \right) \\ = \langle C[\delta f_s] \rangle_{R_s} - \langle \mathbf{V}_E \rangle_{R_s} \cdot \left(\frac{RB_\phi}{B} \frac{m_s w_\parallel}{T_s} F_{0,s} \nabla \Omega_\phi + \nabla F_{0,s} \right), \end{aligned} \tag{A3}$$

in $(R_s, \varepsilon_s, \mu_s, \vartheta)$ coordinates, where $R_s = \mathbf{r} - \boldsymbol{\rho}_s$ is the particle’s gyrocentre, \mathbf{r} is its position, $\varepsilon_s = m_s w^2/2$ is its kinetic energy, $\mu_s = m_s w_\perp^2/2B$ its magnetic moment and ϑ its gyrophase. Here, $\langle \cdot \rangle_{R_s}$ denotes an average over ϑ at fixed R_s , φ is the fluctuating electrostatic potential, w is the particle velocity relative to \mathbf{u} , subscripts \parallel and \perp indicate components along and across \mathbf{B} respectively, $F_{0,s}$ is a local Maxwellian velocity distribution, C is the collision operator and B_ϕ is the toroidal component of \mathbf{B} . The drift velocity due to magnetic curvature and ∇B is $\mathbf{V}_{B,s} = \hat{\mathbf{b}}/\Omega_s \times [w_\perp^2 \nabla \ln(B)/2 + w_\parallel^2 \hat{\mathbf{b}} \cdot \nabla \hat{\mathbf{b}}]$, and the Coriolis drift velocity is $\mathbf{V}_{C,s} = (2w_\parallel \Omega_\phi / \Omega_s) \hat{\mathbf{b}} \times (\hat{\mathbf{z}} \times \hat{\mathbf{b}})$ with $\hat{\mathbf{z}}$ the unit vector in the vertical direction. The nonlinearity in (A3) stems from the fluctuating $\mathbf{E} \times \mathbf{B}$ drift $\mathbf{V}_E = c\hat{\mathbf{b}}/B \times \nabla \varphi$ advecting δf_s on the left-hand side. Perpendicular flow shear enters via the convective time derivative, while the drives from the shear in the parallel flow and the temperature gradient, respectively, enter via the $\nabla \Omega_\phi$ and $\nabla F_{0,s}$ terms on the right-hand side. The temperature gradient is specified by the normalised inverse gradient length $a/L_{T_s} = -a d(\ln T_s)/dr_\psi$. The set of equations is closed by the quasineutrality condition

$$\sum_s Z_s \int d^3 w \langle \delta f_s \rangle_{R_s} = \sum_s \frac{eZ_s^2}{T_s} \left(n_s \varphi - \int d^3 w \langle \varphi \rangle_{R_s} F_{0,s} \right), \tag{A4}$$

where n_s is the particle density and $\langle \cdot \rangle_r$ denotes an average over ϑ at fixed particle position.

Fluctuations with no spatial variation other than in the radial direction are known as ‘zonal’ fluctuations, and produce sheared $\mathbf{E} \times \mathbf{B}$ drifts in the y direction. The zonal flow is given by

$$V_Z = -\frac{c}{B} \hat{\mathbf{b}} \times \nabla r_\psi \Big| \frac{\partial \varphi_Z}{\partial r_\psi}, \tag{A5}$$

where φ_Z is the zonal part of the electrostatic potential. The shear of the zonal flow is $\gamma_Z = \partial V_Z / \partial r_\psi$.

The system of (A3) and (A4) is solved for δf_s and φ using the local gyrokinetic code GS2 (Kotschenreuther *et al.* 1995; Barnes *et al.* 2009; Highcock 2012; Christen *et al.* 2021) in a filament-like simulation domain (known as a flux tube Beer *et al.* 1995) that follows a magnetic field line around the flux surface of interest. The flux-surface label $x = (q_0/r_{\psi,0}B_r)(\psi - \psi_0)$ and the field-line label $y = (1/B_r)(\partial\psi/\partial r_{\psi})|_{r_{\psi,0}}(\alpha - \alpha_0)$ are used as coordinates across \mathbf{B} . The poloidal angle θ serves as the coordinate along \mathbf{B} . Here, B_r is a reference magnetic field strength, $\psi = \int_0^r dr' r' R \mathbf{B} \cdot \nabla \theta$ is the poloidal magnetic flux, r is the minor radius of the torus and $\alpha = \phi - \int_0^\theta d\theta' (\mathbf{B} \cdot \nabla \phi) / (\mathbf{B} \cdot \nabla \theta)|_\psi$ labels field lines on a given flux surface. The code computes the turbulent contribution to the heat and momentum fluxes given by

$$Q_s = \left\langle \int d^3 \mathbf{w} \frac{m_s w^2}{2} \delta f_s V_E \cdot \nabla \psi \right\rangle_\psi, \quad (\text{A6})$$

$$\Pi_s = \left\langle m_s R^2 \int d^3 \mathbf{v} (\mathbf{v} \cdot \nabla \phi) \delta f_s V_E \cdot \nabla \psi \right\rangle_\psi, \quad (\text{A7})$$

respectively, with $\langle \cdot \rangle_\psi$ denoting the volume average over the flux tube.

Appendix B. Correlation time and correlation lengths

Given a saturated turbulent state, we estimate the eddy correlation time as being

$$\tau = \left[\frac{c}{B} \frac{[\varphi_{\text{NZ}}]_{\text{rms}}}{\ell_x \ell_y} \right]^{-1}, \quad (\text{B1})$$

where ℓ_x and ℓ_y denote the eddy correlation length in the x and y directions, respectively, and where $[\varphi_{\text{NZ}}]_{\text{rms}} = \sqrt{\langle \varphi_{\text{NZ}}^2 \rangle_{t,x,y}}$ is the root mean square of the non-zonal part of the electrostatic potential φ_{NZ} , averaged over time, x and y . The expression (B1) is obtained from the nonlinear term in the gyrokinetic equation (A3). We then define the two-point spatial correlation function

$$\text{Cor}[\varphi](\delta_x, \delta_y) = \frac{\langle \varphi(t, x, y) \varphi(t, x + \delta_x, y + \delta_y) \rangle_{t,x,y}}{\langle \varphi^2(t, x, y) \rangle_{t,x,y}^{1/2} \langle \varphi^2(t, x + \delta_x, y + \delta_y) \rangle_{t,x,y}^{1/2}}. \quad (\text{B2})$$

The correlation lengths ℓ_x and ℓ_y are chosen to correspond to the e -folding of $\text{Cor}[\varphi_{\text{NZ}}]$ along the δ_x direction (adjusted to match the tilt induced by the flow shear) and the δ_y direction, respectively. Typical examples of $\text{Cor}[\varphi_{\text{NZ}}]$ are shown in figure 7. The zonal correlation length $\ell_{x,z}$ corresponds to the e -folding of $\text{Cor}[\varphi_Z]$ along the δ_x direction. Note that the exact definition of the correlation lengths is somewhat arbitrary. Another choice, that is commonly found in the literature, is to define ℓ_x and ℓ_y as the integral of $\text{Cor}[\varphi_{\text{NZ}}]$ along the δ_x and δ_y axes – which, in our case, yields similar results to the e -folding lengths.

Appendix C. Source code

The version of the GS2 code used for this work is available at https://bitbucket.org/gyrokinetics/gs2/branch/ndc_branch, with the newest commit at the time of writing being 0abdcd. The associated version of ‘Makefiles’ necessary for compilation is available at https://bitbucket.org/gyrokinetics/makefiles/branch/ndc_branch under the commit ba24979, and the additional ‘utils’ files required to run the code are available at https://bitbucket.org/gyrokinetics/utills/branch/ndc_branch under the commit 8e41f9a.

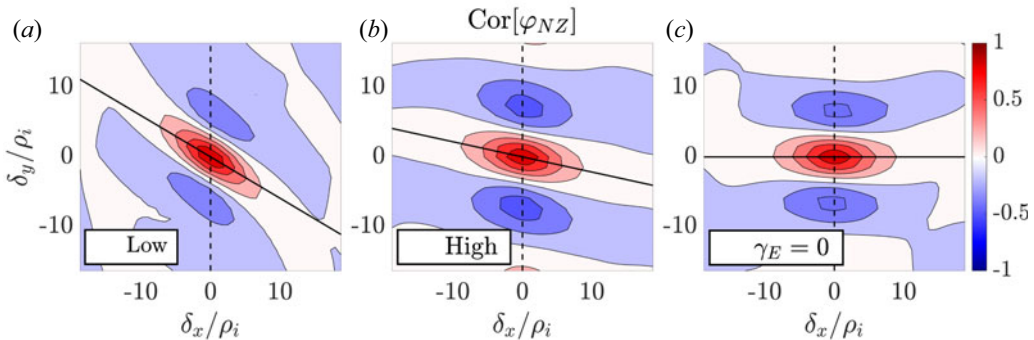


FIGURE 7. Two-point spatial correlation function for a low-transport state (a), a high-transport state (b) and a state with no mean flow shear (c). For the three states, $a/L_T_i = 1.76$. In (a,b), $\gamma_E = -0.079$.

REFERENCES

- ABEL, I., PLUNK, G., WANG, E., BARNES, M., COWLEY, S., DORLAND, W. & SCHEKOCHIHIN, A. 2013 Multiscale gyrokinetics for rotating tokamak plasmas: fluctuations, transport and energy flows. *Rep. Prog. Phys.* **76** (11), 116201.
- ARTUN, M. & TANG, W.M. 1992 Gyrokinetic analysis of ion temperature gradient modes in the presence of sheared flows. *Phys. Fluids B* **4** (5), 1102–1114.
- BARNES, M., ABEL, I.G., DORLAND, W., ERNST, D.R., HAMMETT, G.W., RICCI, P., ROGERS, B.N., SCHEKOCHIHIN, A.A. & TATSUNO, T. 2009 Linearized model Fokker–Planck collision operators for gyrokinetic simulations. II. Numerical implementation and tests. *Phys. Plasmas* **16** (7), 072107.
- BARNES, M., PARRA, F.I., HIGHCOCK, E.G., SCHEKOCHIHIN, A.A., COWLEY, S.C. & ROACH, C.M. 2011 Turbulent transport in tokamak plasmas with rotational shear. *Phys. Rev. Lett.* **106**, 175004.
- BEER, M.A., COWLEY, S. & HAMMETT, G. 1995 Field-aligned coordinates for nonlinear simulations of tokamak turbulence. *Phys. Plasmas* **2** (7), 2687–2700.
- BELLI, E.A. 2006 Studies of numerical algorithms for gyrokinetics and the effects of shaping on plasma turbulence. PhD thesis, Princeton University.
- BIGLARI, H., DIAMOND, P.H. & TERRY, P.W. 1990 Influence of sheared poloidal rotation on edge turbulence. *Phys. Fluids B* **2** (1), 1–4.
- BURGGRAF, O.R. & FOSTER, M.R. 1977 Continuation or breakdown in tornado-like vortices. *J. Fluid Mech.* **80** (4), 685–703.
- CASSON, F.J., PEETERS, A.G., CAMENEN, Y., HORNSBY, W.A., SNODIN, A.P., STRINTZI, D. & SZEPESI, G. 2009 Anomalous parallel momentum transport due to ExB flow shear in a tokamak plasma. *Phys. Plasmas* **16** (9), 092303.
- CATTO, P.J. 1978 Linearized gyro-kinetics. *Plasma Phys.* **20** (7), 719–722.
- CATTO, P.J., BERNSTEIN, I.B. & TESSAROTTO, M. 1987 Ion transport in toroidally rotating tokamak plasmas. *Phys. Fluids* **30** (9), 2784–2795.
- CHANDRARAJAN JAYALEKSHMI, A. 2020 Studying the effect of non-adiabatic passing electron dynamics on microturbulence self-interaction in fusion plasmas using gyrokinetic simulations. PhD thesis, École Polytechnique Fédérale de Lausanne.
- CHRISTEN, N., BARNES, M. & PARRA, F. 2021 Continuous-in-time approach to flow shear in a linearly implicit local delta-f gyrokinetic code. *J. Plasma Phys.* **87** (2), 905870230.
- COLYER, G.J., SCHEKOCHIHIN, A.A., PARRA, F.I., ROACH, C.M., BARNES, M.A., GHIM, Y.-C. & DORLAND, W. 2017 Collisionality scaling of the electron heat flux in ETG turbulence. *Plasma Phys. Control. Fusion* **59** (5), 055002.
- CONNOR, J.W. 1998 A review of models for ELMs. *Plasma Phys. Control. Fusion* **40** (2), 191–213.
- COWLEY, S.C., KULSRUD, R.M. & SUDAN, R. 1991 Considerations of ion-temperature-gradient-driven turbulence. *Phys. Fluids B* **3** (10), 2767–2782.

- DIAMOND, P.H., ITOH, S., ITOH, K. & HAHM, T. 2005 Zonal flows in plasma—a review. *Plasma Phys. Control. Fusion* **47** (5), R35.
- DIMITS, A.M., BATEMAN, G., BEER, M.A., COHEN, B.I., DORLAND, W., HAMMETT, G.W., KIM, C., KINSEY, J.E., KOTSCHENREUTHER, M., KRITZ, A.H., *et al.* 2000 Comparisons and physics basis of tokamak transport models and turbulence simulations. *Phys. Plasmas* **7** (3), 969–983.
- DIMITS, A.M., WILLIAMS, T.J., BYERS, J.A. & COHEN, B.I. 1996 Scalings of ion-temperature-gradient-driven anomalous transport in tokamaks. *Phys. Rev. Lett.* **77**, 71–74.
- FAISST, H. & ECKHARDT, B. 2004 Sensitive dependence on initial conditions in transition to turbulence in pipe flow. *J. Fluid Mech.* **504**, 343–352.
- FOX, M.F.J., VAN WYK, F., FIELD, A.R., GHIM, Y.-C., PARRA, F.I. & SCHEKOCIHIN, A.A. 2017 Symmetry breaking in MAST plasma turbulence due to toroidal flow shear. *Plasma Phys. Control. Fusion* **59** (3), 034002.
- FRIEMAN, E.A. & CHEN, L. 1982 Nonlinear gyrokinetic equations for low-frequency electromagnetic waves in general plasma equilibria. *Phys. Fluids* **25** (3), 502–508.
- VON GOELER, S., STODIEK, W. & SAUTHOFF, N. 1974 Studies of internal disruptions and $m = 1$ oscillations in tokamak discharges with soft-X-ray techniques. *Phys. Rev. Lett.* **33**, 1201–1203.
- HAMMETT, G.W., DORLAND, W., LOUREIRO, N.F. & TATSUNO, T. 2006 Implementation of large scale $E \times B$ shear flow in the gs2 gyrokinetic turbulence code. In *Poster Presented at the DPP Meeting of the American Physical Society*.
- HASTIE, R. 1997 Sawtooth instability in tokamak plasmas. *Astrophys. Space Sci.* **256** (1), 177–204.
- HIGHCOCK, E. 2012 The zero-turbulence manifold in fusion plasmas. PhD thesis, Oxford University, UK.
- HIGHCOCK, E.G., BARNES, M., PARRA, F.I., SCHEKOCIHIN, A.A., ROACH, C.M. & COWLEY, S.C. 2011 Transport bifurcation induced by sheared toroidal flow in tokamak plasmas. *Phys. Plasmas* **18** (10), 102304.
- HIGHCOCK, E.G., BARNES, M., SCHEKOCIHIN, A.A., PARRA, F.I., ROACH, C.M. & COWLEY, S.C. 2010 Transport bifurcation in a rotating tokamak plasma. *Phys. Rev. Lett.* **105**, 215003.
- HIGHCOCK, E., SCHEKOCIHIN, A., COWLEY, S., BARNES, M., PARRA, F., ROACH, C. & DORLAND, W. 2012 Zero-turbulence manifold in a toroidal plasma. *Phys. Rev. Lett.* **109** (26), 265001.
- IVANOV, P.G., SCHEKOCIHIN, A.A., DORLAND, W., FIELD, A.R. & PARRA, F.I. 2020 Zonally dominated dynamics and dimits threshold in curvature-driven ITG turbulence. *J. Plasma Phys.* **86** (5), 855860502.
- KOTSCHENREUTHER, M., REWOLDT, G. & TANG, W.M. 1995 Comparison of initial value and eigenvalue codes for kinetic toroidal plasma instabilities. *Comput. Phys. Commun.* **88** (2), 128–140.
- LATTER, H.N. & PAPALOIZOU, J.C.B. 2012 Hysteresis and thermal limit cycles in MRI simulations of accretion discs. *Mon. Not. R. Astron. Soc.* **426** (2), 1107–1120.
- MANTICA, P., STRINTZI, D., TALA, T., GIROUD, C., JOHNSON, T., LEGGATE, H., LERCHE, E., LOARER, T., PEETERS, A.G., SALMI, A., *et al.* 2009 Experimental study of the ion critical-gradient length and stiffness level and the impact of rotation in the JET tokamak. *Phys. Rev. Lett.* **102**, 175002.
- MCMILLAN, B.F., BALL, J. & BRUNNER, S. 2019 Simulating background shear flow in local gyrokinetic simulations. *Plasma Phys. Control. Fusion* **61** (5), 055006.
- MCMILLAN, B.F., JOLLIET, S., TRAN, T., VILLARD, L., BOTTINO, A. & ANGELINO, P. 2009 Avalanchelike bursts in global gyrokinetic simulations. *Phys. Plasmas* **16** (2), 022310.
- MCMILLAN, B.F., PRINGLE, C.C.T. & TEACA, B. 2018 Simple advecting structures and the edge of chaos in subcritical tokamak plasmas. *J. Plasma Phys.* **84** (6), 905840611.
- PARRA, F.I., BARNES, M., HIGHCOCK, E.G., SCHEKOCIHIN, A.A. & COWLEY, S.C. 2011 Momentum injection in tokamak plasmas and transitions to reduced transport. *Phys. Rev. Lett.* **106**, 115004.
- PEETERS, A.G., RATH, F., BUCHHOLZ, R., CAMENEN, Y., CANDY, J., CASSON, F.J., GROSSHAUSER, S.R., HORNSBY, W.A., STRINTZI, D. & WEIKL, A. 2016 Gradient-driven flux-tube simulations of ion temperature gradient turbulence close to the non-linear threshold. *Phys. Plasmas* **23** (8), 082517.
- PUESCHEL, M.J., KAMMERER, M. & JENKO, F. 2008 Gyrokinetic turbulence simulations at high plasma beta. *Phys. Plasmas* **15** (10), 102310.
- RAVELET, F., MARIÉ, L., CHIFFAUDEL, A. & DAVIAUD, F. 2004 Multistability and memory effect in a highly turbulent flow: experimental evidence for a global bifurcation. *Phys. Rev. Lett.* **93** (16), 164501.

- REMPEL, E.L., LESUR, G. & PROCTOR, M.R.E. 2010 Supertransient magnetohydrodynamic turbulence in Keplerian shear flows. *Phys. Rev. Lett.* **105**, 044501.
- ROGERS, B.N., DORLAND, W. & KOTSCHENREUTHER, M. 2000 Generation and stability of zonal flows in ion-temperature-gradient mode turbulence. *Phys. Rev. Lett.* **85**, 5336–5339.
- ROMANELLI, F. 1989 Ion temperature-gradient-driven modes and anomalous ion transport in tokamaks. *Phys. Fluids B* **1** (5), 1018–1025.
- SCHEKOCIHIN, A.A., HIGHCOCK, E.G. & COWLEY, S.C. 2012 Subcritical fluctuations and suppression of turbulence in differentially rotating gyrokinetic plasmas. *Plasma Phys. Control. Fusion* **54** (5), 055011.
- SCHMUCKER, A. & GERSTEN, K. 1988 Vortex breakdown and its control on delta wings. *Fluid Dyn. Res.* **3** (1–4), 268–272.
- SHAFER, M.W., FONCK, R.J., MCKEE, G.R., HOLLAND, C., WHITE, A.E. & SCHLOSSBERG, D.J. 2012 2D properties of core turbulence on DIII-D and comparison to gyrokinetic simulations. *Phys. Plasmas* **19** (3), 032504.
- SHTERN, V. & HUSSAIN, F. 1993 Hysteresis in a swirling jet as a model tornado. *Phys. Fluids A* **5** (9), 2183–2195.
- SIMITEV, R.D. & BUSSE, F.H. 2009 Bistability and hysteresis of dipolar dynamos generated by turbulent convection in rotating spherical shells. *Europhys. Lett.* **85** (1), 19001.
- SIREN, P., VARJE, J., WEISEN, H. & GIACOMELLI, L. 2019 Role of JETPEAK database in validation of synthetic neutron camera diagnostics and ASCOT- AFSI fast particle and fusion product calculation chain in JET. *J. Instrum.* **14** (11), C11013–C11013.
- SNEDEKER, R.S. & DONALDSON, C.D. 1966 Observation of a bistable flow in a hemispherical cavity. *AIAA J.* **4** (4), 735–736.
- SUGAMA, H. & HORTON, W. 1998 Nonlinear electromagnetic gyrokinetic equation for plasmas with large mean flows. *Phys. Plasmas* **5** (7), 2560–2573.
- SYNAKOWSKI, E.J., BATHA, S.H., BEER, M.A., BELL, M.G., BELL, R.E., BUDNY, R.V., BUSH, C.E., EFTHIMION, P.C., HAMMETT, G.W., HAHM, T.S., *et al.* 1997 Roles of electric field shear and Shafranov shift in sustaining high confinement in enhanced reversed shear plasmas on the TFTR tokamak. *Phys. Rev. Lett.* **78**, 2972–2975.
- WALBROECK, F.L. & CHEN, L. 1991 Ballooning instabilities in tokamaks with sheared toroidal flows. *Phys. Fluids B* **3** (3), 601–610.
- WAGNER, F., BECKER, G., BEHRINGER, K., CAMPBELL, D., EBERHAGEN, A., ENGELHARDT, W., FUSSMANN, G., GEHRE, O., GERNHARDT, J., GIERKE, G.V., *et al.* 1982 Regime of improved confinement and high beta in neutral-beam-heated divertor discharges of the ASDEX tokamak. *Phys. Rev. Lett.* **49**, 1408–1412.
- WEIKL, A., PEETERS, A.G., RATH, F., GROSSHAUSER, S.R., BUCHHOLZ, R., HORNSBY, W.A., SEIFERLING, F. & STRINTZI, D. 2017 Ion temperature gradient turbulence close to the finite heat flux threshold. *Phys. Plasmas* **24** (10), 102317.
- VAN WYK, F., HIGHCOCK, E.G., FIELD, A.R., ROACH, C.M., SCHEKOCIHIN, A.A., PARRA, F.I. & DORLAND, W. 2017 Ion-scale turbulence in MAST: anomalous transport, subcritical transitions, and comparison to BES measurements. *Plasma Phys. Control. Fusion* **59** (11), 114003.
- VAN WYK, F., HIGHCOCK, E.G., SCHEKOCIHIN, A.A., ROACH, C.M., FIELD, A.R. & DORLAND, W. 2016 Transition to subcritical turbulence in a tokamak plasma. *J. Plasma Phys.* **82** (6), 905820609.